Latest developments in Automotive Aerodynamics using LS-DYNA®

Iñaki Çaldichoury[1*], Facundo Del Pin[1], Rodrigo Paz[1]
[1] *Livermore Software Technology Corporation, Livermore, CA, USA*
**Corresponding author. Email: inaki@lstc.com*

Abstract

LS-DYNA® is a general purpose explicit and implicit finite element program used to analyse the non-linear dynamic response of three-dimensional solids and fluids. It is developed by Livermore Software Technology Corporation (LSTC). A module to simulate incompressible flows has been added to LS-DYNA® for coupled fluid/mechanical/thermal simulations (ICFD solver). It offers a response to the ever increasing need of engineers in the automotive industry sector and elsewhere to comprehend and solve complex highly nonlinear problems involving multiple domains of physics. However, if the ICFD solver is to become a viable proposition in automotive aerodynamics, it must demonstrate its ability to accurately reproduce the elementary phenomena observed on simple geometric forms in the wind tunnel. With this objective in mind, the present paper will show for different wind speeds what results can be obtained on widely studied simplified car geometry, the Ahmed body, focusing on the complex 25° slant degree case.

Keywords

Computational fluid dynamics (CFD), turbulent flow (RANS), Ahmed body, Multiphysics,

1 Introduction

The geometry that this paper will focus on is derived from the work of (Ahmed, Ramm and Faltin 1984). It features a simplified geometry of a car that would have been stripped of all its external features (mirrors, tires etc). The front of the body is smoothed out so as to prevent any turbulent disturbance coming from the front affecting the rear part (See **Fig. 1**). (Ahmed, Ramm and Faltin 1984) varied the slant angle and identified three flow regimes and drag coefficient behaviour (see **Fig. 2**). For angles below 12.5° the flow on the slant remains largely attached separating only at the base area resulting in low drag values. As the angle increases the flow starts to display more complex 3D features, with

two recirculating eddies at the base area, two counter rotating longitudinal vortices starting at the lateral edges of the slant and moving towards the centre line in the wake. In the highest angles, a separation bubble forms on the slant. The drag then quickly increases until it reaches the critical angle of 30° where a complete separation of the flow at the intersection between slant and body occurs resulting in an abrupt decrease in drag.

In the present paper, we will focus on the 25° slant angle. This particular angle has been heavily studied both experimentally and numerically due to its complexity. (Bayraktar, Landman and Baysal 2001), (Meile, et al. 2011), (Gilleron and Chometon 1999) have all tried different Reynolds numbers but their results showed consistency with the original work of (Ahmed, Ramm and Faltin 1984). (Conan, Anthoine and Planquart 2011), (Leclerc 2008) and (Thacker, et al. 2012) however showed results that were systematically above the commonly adopted values. (Leclerc 2008) attributes the higher drag values to the formation of a local separation bubble on the slant. Under these considerations, the results presented by (Thacker, et al. 2012) are especially interesting. In their work, two configurations are studied. One with a sharp edge at the transition between the body and the slant, the other with a more rounded geometry. In the case of the sharp edge, the bubble is indeed present and his drag results are consistent with those of (Leclerc 2008). In the rounded edge configuration, the bubble is not present and his results are consistent with those of (Conan, Anthoine and Planquart 2011) and closer to those of (Ahmed, Ramm and Faltin 1984). During our numerical analysis, the behaviour of the flow over the slant will be of particular interest as it seems to have a big impact on the total drag.

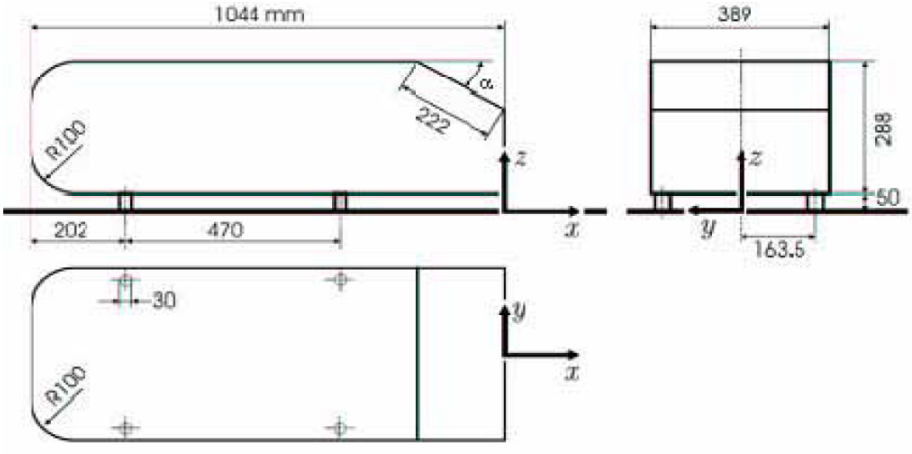

***Figure 1**: Ahmed body geometry and dimensions*

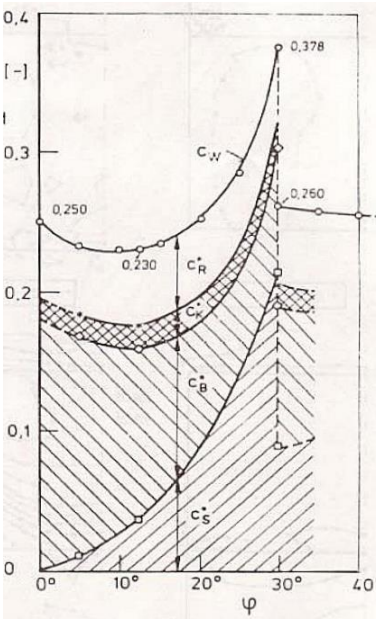

***Figure 2**: Drag Coefficient function of slant angle for $Re = 4.2e^6$. Cs, Cb, Ck, Cr and Cw are the slant, back, front, friction and total drag coefficients respectfully. Results by (Ahmed, Ramm and Faltin 1984).*

2 Numerical analysis set up

For the numerical analysis, the ICFD solver included in LS-DYNA® will be used. The ICFD solver uses a two-step Taylor-Galerkin fractional-step finite element method, which is of second order accuracy (See (Codina 2001) and (Del Pin, Çaldichoury and Paz 2011)). It features several turbulence models (Standard k-Epsilon, LES-Smagorinsky, LES-Wale). In its latest release it also includes some $k-\omega$ models as well as the realizable $k-\varepsilon$ turbulence model which is considered to be an improvement over the standard model (See (Shih, et al. 1995)) and which will be used here. The standard characteristic of air will be chosen for the density ($\rho = 1.225\, kg/m^3$) and the viscosity ($\mu = 1.78e^{-5} Pa.s$) and the incoming velocity will be varied from $10\, m/s$ to $120\, m/s$ thus covering a wide range of Reynolds numbers based on the length of the body ($L = 1.044\, m$). The drag coefficient will be calculated using the projected front area as reference area ($A_{front} = 0.112032\, m^2$).

Furthermore, the ICFD solver makes use of powerful automatic mesh generator that will generate the mesh only leaving to the user the responsibility of providing good quality water tight surface meshes. For our choice of surface mesh size, we will refer to the Taylor scale ((Franck, et al. n.d.)), $l = 15^{0.5} A^{-0.5} Re^{-0.5} L$, $A = 0.5$, that gives values between 0.007 and 0.002 depending on the Reynolds number. We will adopt the intermediate values of 0.006 on the slant and 0.002 on the front. Regarding the Boundary layer mesh, the solver provides tools to control for the total height, the location of the first node as well as the growth rate. In order to estimate a Y+ value, we base ourselves on the results for a

flat plate (See (White n.d.)). To maintain a Y+ value of 30, the first element needs to have a size between $1e^{-3}$ and $1e^{-4}$ depending on the Reynolds number. For all the runs, we will choose the most conservative value of $1e^{-4}$ and put ten elements in the boundary layer mesh by using a constant growth method. The generated mesh consists of approximately $9M$ elements. **Fig. 3** and **Fig. 4** offer a global view of the domain as well as a zoom in of the resulting mesh over the slant.

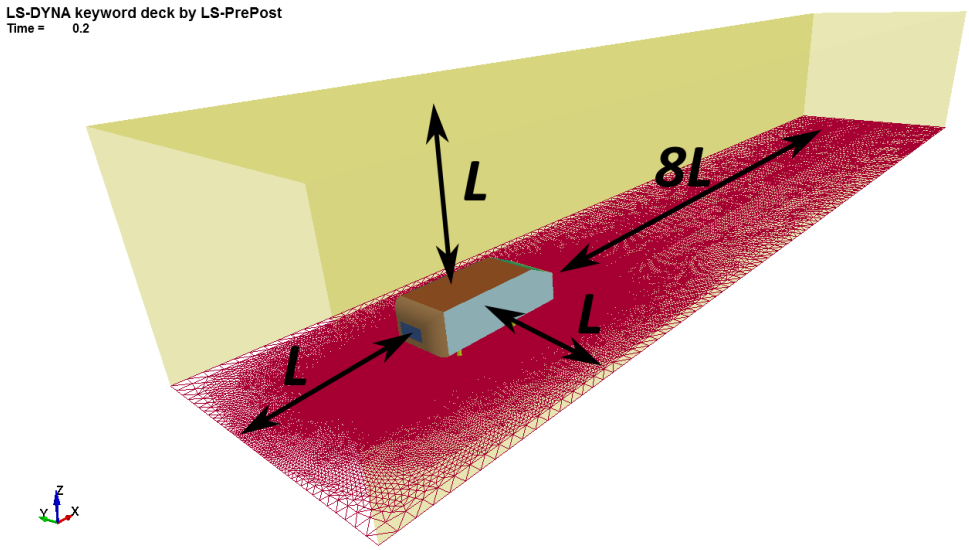

***Figure 3**: Dimensions of the bounding box function of reference Ahmed body length* $L = 1.044m$

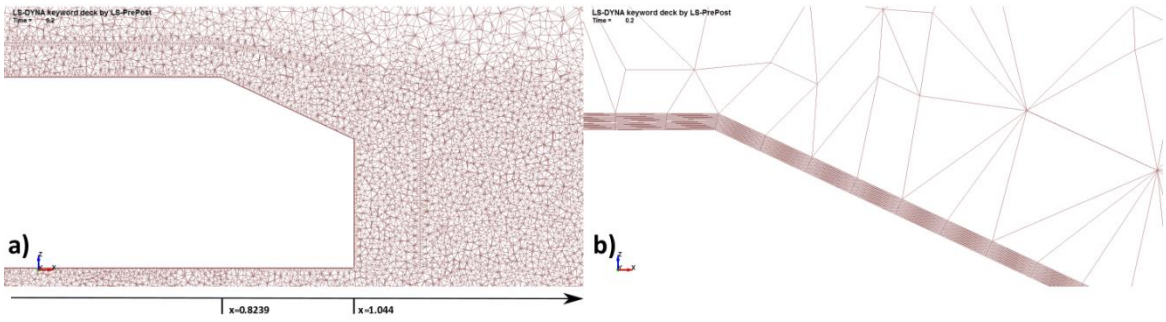

***Figure 4**: Generated mesh focus on a) the slant area and b) the intersection between body and slant*

The runs will be conducted using the ICFD transient solver. During our first trials, it has been discovered that the stability of the analysis was sensitive to the value of the timestep. A timestep that had a local CFL number higher than 100 in the boundary layer mesh often resulted in instabilities. For each run, based on the inflow velocity, we will

therefore slightly adjust the timestep . For example, for an inflow velocity of $40\ m/s$ and a mesh size $dx = 1e^{-4}$, we will pick $dt = \frac{dx}{V} \times 20 = 5e^{-5}$ based to the assumption that having a local CFL number of 20 in certain areas is considered acceptable. Since the analysis will be made using a transient solver, one must decide on a convergence criteria. In our case the analysis will be deemed as having converged after an imaginary particle coming from the inflow has passed the body five times resulting in 5000 iterations for each case. The drag values will then be computed using an averaged value between iteration 5000 and 6000. **Tab. 1** sums up the chosen timestep for the different Reynolds numbers and the different endtimes.

Velocity (m/s)	Timestep (s)	Endtime (s)
10	$2.0e^{-4}$	1.2
20	$1.0e^{-4}$	0.6
30	$6.67e^{-5}$	0.4
40	$5.0e^{-5}$	0.3
60	$3.33e^{-5}$	0.2
80	$2.5e^{-5}$	0.15
100	$2.0e^{-5}$	0.12
120	$1.15e^{-5}$	0.1

***Table 1**: Time step choice function of inflow velocity*

3 Results and discussion

Fig. 5 shows the drag behaviour for the different Reynolds numbers. As can be observed, the chosen value of 5000 iterations proved to be quite conservative, many of the runs with lower speeds runs may be considered as having converged sooner. **Fig. 6** shows the Y+ on the body for different Reynolds numbers. As was expected, the Y+ remains in the vicinity of 30 with the highest values being at the front where the velocity is greatest.

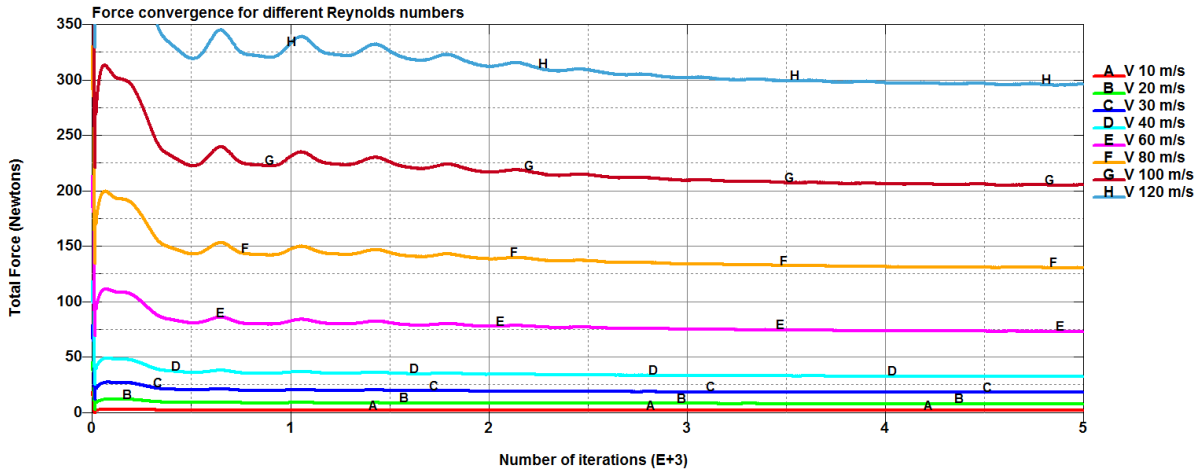

***Figure 5**: Total Force convergence function of the number of iterations for different inflow velocities.*

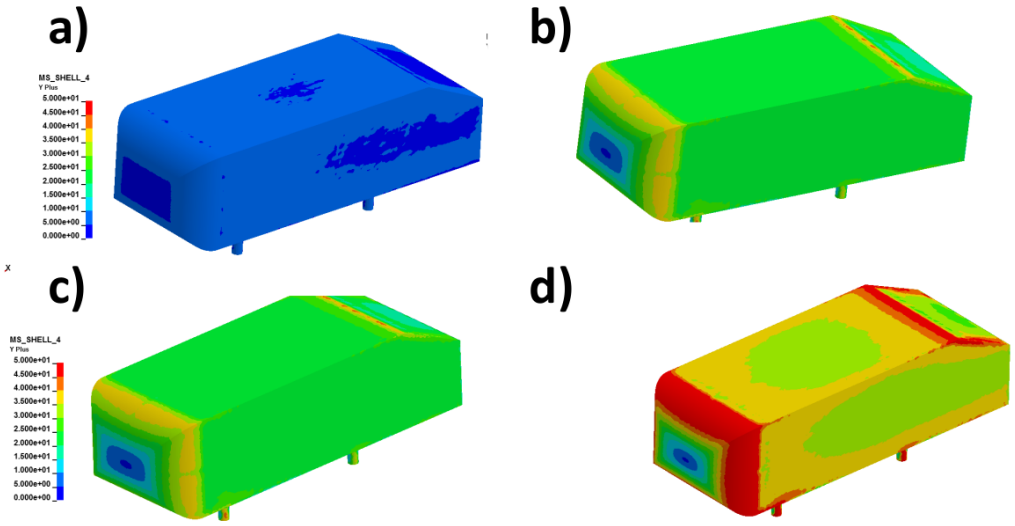

***Figure 6**: Y+ on the whole body for different inflow velocities a) $V = 10\ m/s$, b) $V = 40\ m/s$, c) $V = 60\ m/s$, d) $V = 100\ m/s$ and same fringe range going from 0 to 50.*

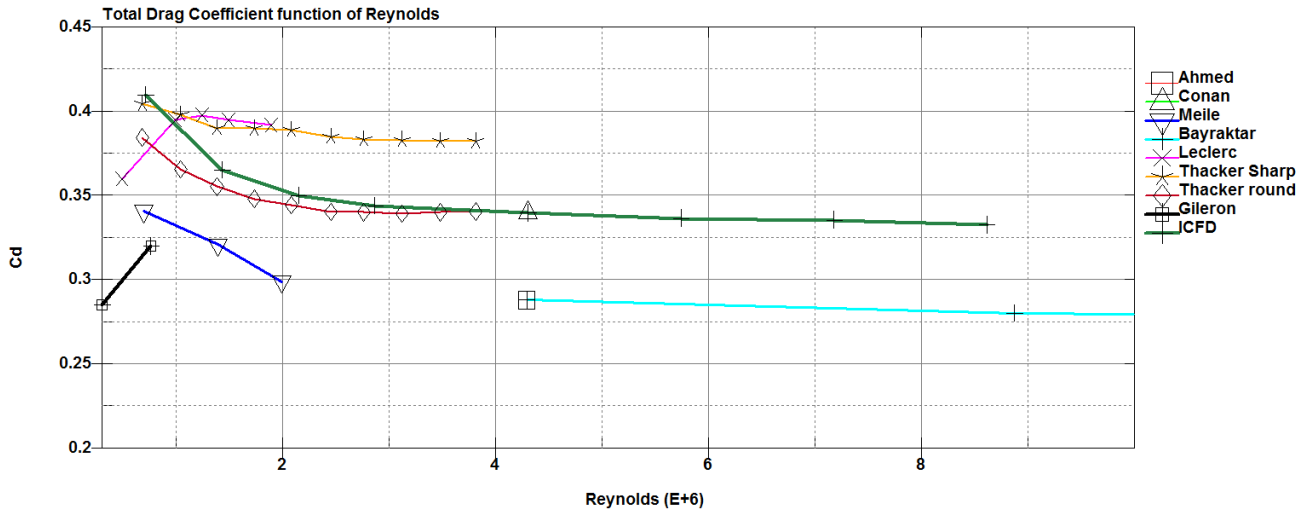

***Figure 7**: Comparison between the present numerical analysis using the ICFD solver and different experimental results for the total drag coefficient.*

Fig. 7 offers a comparison between current results for the total drag coefficient ($C_d = F/(0.5\rho V^2 A_{front})$) and some experimental references. The global expected behaviour is correctly captured with the drag coefficient decreasing as the Reynolds number increases, finally converging for an almost constant value of 0.34 around $Re = 2.5e^6$. Although not shown here, lift is also correctly captured, with an almost constant lift coefficient of 0.42 which is good agreement with the results of (Thacker, et al. 2012) and (Gilleron and Chometon 1999). Considering the wide discrepancies of the experimental results concerning the drag coefficient, let us now try to characterize the flow in the wake and on the slant in order to better understand the flow phenomena. If we focus on the $Re = 4.3e^6$ case, and look at the wake flow on **Fig. 8**, we can see that the flow remains completely attached with no local separation bubble but two toric structures located one above the other $10\ cm$ after the end of the body approximatively. This is the exact flow structure reported by (Thacker, et al. 2012) in his "rounded edge configuration". This explains our lower drag values than those reported by (Leclerc 2008) and (Thacker, et al. 2012) in the sharp edge configuration. In both cases, the separation bubble was identified which resulted in a big increase in drag. It is not exactly clear in the original paper of Ahmed if the bubble was present in their $25°$ configuration. It is only reported that local separation occurs in the "higher angle configurations". Therefore we'll look at experimental results that reported close agreement to those of (Ahmed, Ramm and Faltin 1984). **Fig. 9** shows the flow vector in different planes behind the body. Close agreement is found with the turbulent structures reported by (Lienhart, Stoots and Becker n.d.). The longitunal vortexes are also correctly captured (See **Fig. 10**). The pressure mapping across the slant is displayed in **Fig. 11**. Again the influence of the side vortexes is felt with a less dramatic increase in the pressure close to the edges. Let us now look at the pressure coefficient ($C_p = (P - P_{ref})/(0.5\rho V^2)$) across the middle plane on the slant. The present

numerical results again agree very well with the (Thacker, et al. 2012) round edge configuration but also with the (Bayraktar, Landman and Baysal 2001) results. The (Thacker, et al. 2012) sharp edge configuration however has a distinct initial slope that indicates that a separation bubble is present. From there, it can be deduced that in (Bayraktar, Landman and Baysal 2001) experiments, probably no separation bubble was present or it would have shown in his pressure coefficient results.

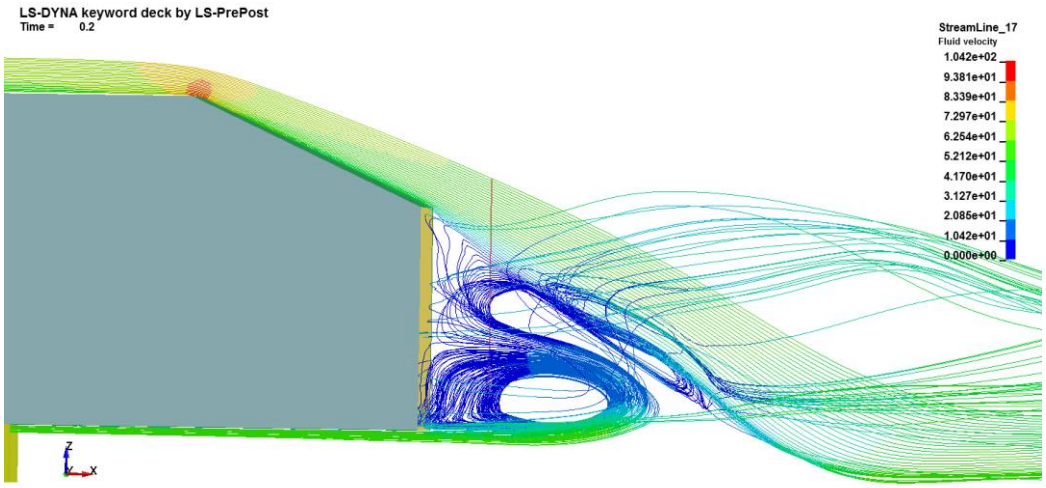

***Figure 8**: Streamlines starting from the middle plane and going over the slant for $V = 60\ m/s$.*

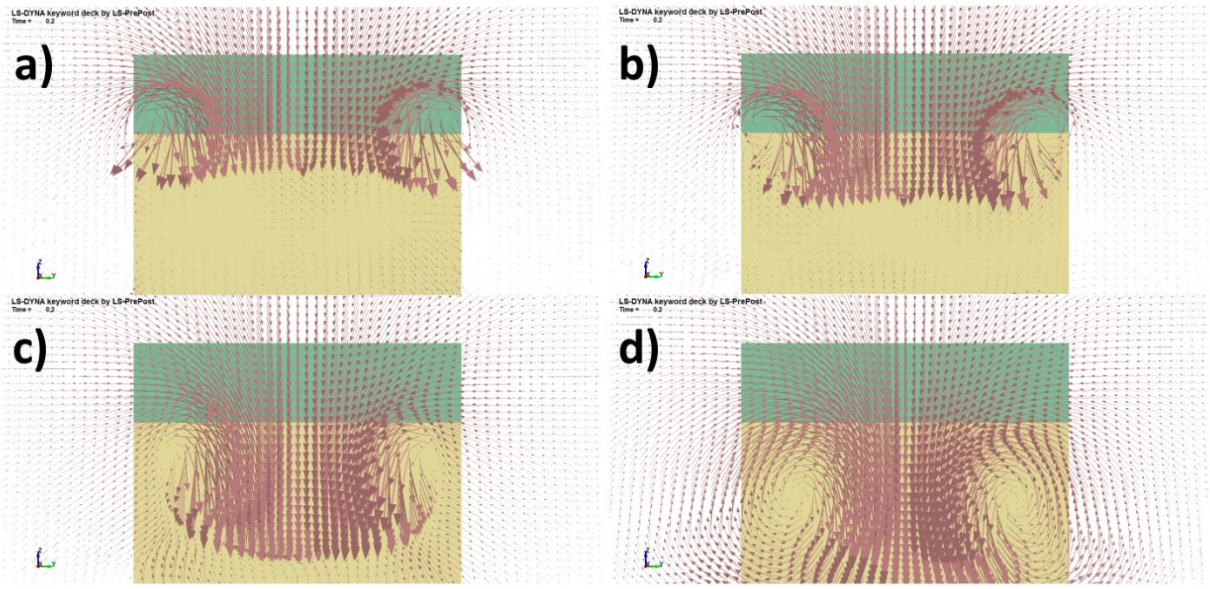

***Figure 9**: Development of the counter-rotating trailing vortex system within the wake of the 25° slant Ahmed body. Average fluid vector visualization at different locations in the wake of the body ($x = 0$), a) $x = 0.01$, b) $x = 0.08$, c) $x = 0.2$, d) $x = 0.8$*

***Figure 10**: Streamlines highlighting the two side vortexes that start close to the edge and move inwards.*

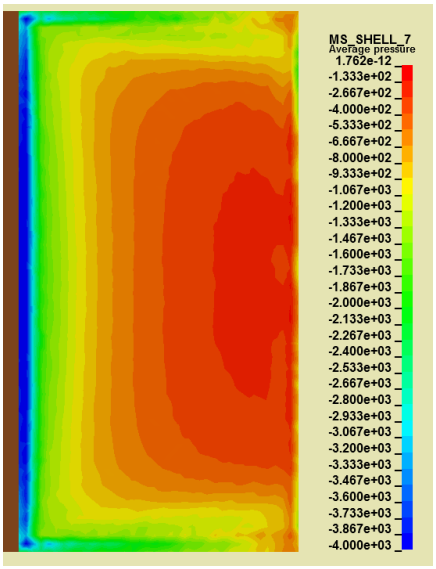

***Figure 11**: Average pressure mapping on the slant for the $V = 60\ m/s$ case.*

It is now clear that the presence and probably the size of a separation bubble on the slant is what separates the experimental data that give a drag coefficient over $Cd = 0.35$ and the other ones that show lower values. The present drag results agree very well with the (Conan, Anthoine and Planquart 2011) and (Thacker, et al. 2012) in the round edge configuration but are still slightly above the results reported by (Ahmed, Ramm and Faltin 1984) and others. **Fig. 14** might give us a precious clue in order to understand better where the differences might be both in the simulation and in the experiments. Indeed, in our numerical results, the drag on the slant and the back increase while the friction drag decreases but even in the higher Reynols number cases, friction still accounts for about 21% of the total drag when Ahmed and all reported that it should be closer to 15%. In fact, our drag results for the back and the slant are in very close agreement with the results reported by (Ahmed, Ramm and Faltin 1984) (less than 10% error). Almost half of the total drag difference can be attributed to the friction, the other big part being the pressure drag on the front part of the body. What most likely happens is that the friction is overestimated in the numerical model which slows down the flow going over the front part of the body. This, in turn, yields a higher pressure which increases the total pressure drag of the front part. In experiments, it can be speculated that something similar occurs. Since (Thacker, et al. 2012) have shown that the slightest change in geometry can cause drastic differences in the drag forces, it is not farfetched to think that slight geometry changes at the front part or even the type of material and rugosity used for the model conception can cause different friction results and therefore might explain why some small discrepancies remain in experimental results even when no separation occurs on the slant.

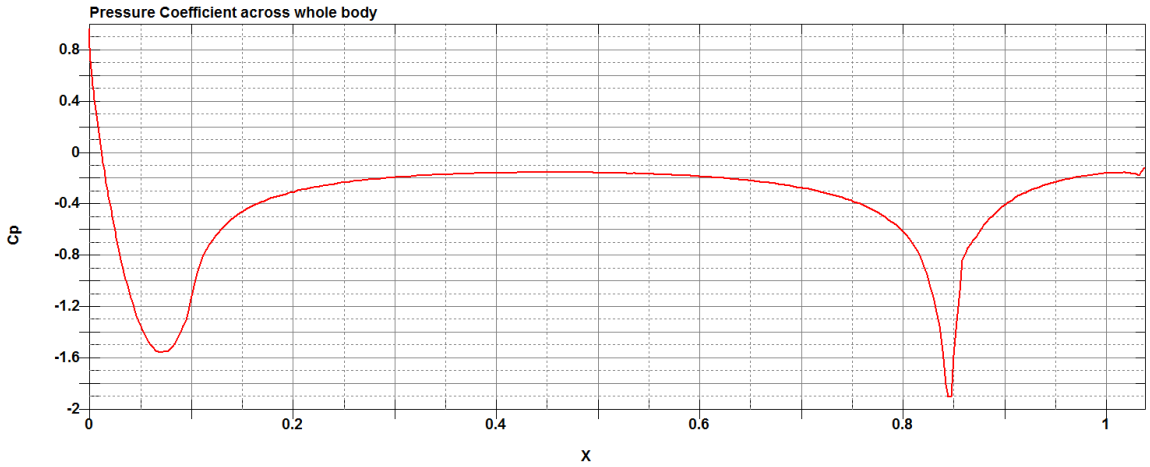

***Figure 12**: Pressure coefficient along the whole upper part of the body in the middle plane for the $V = 60\ m/s$ case*

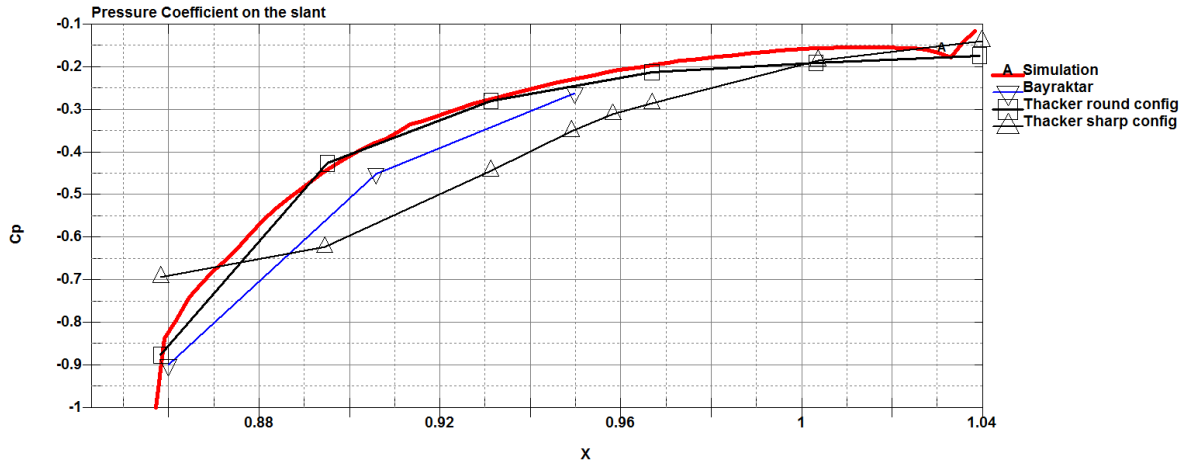

***Figure 13**: Pressure coefficient over the slant. Comparison between the simulation at some experimental results.*

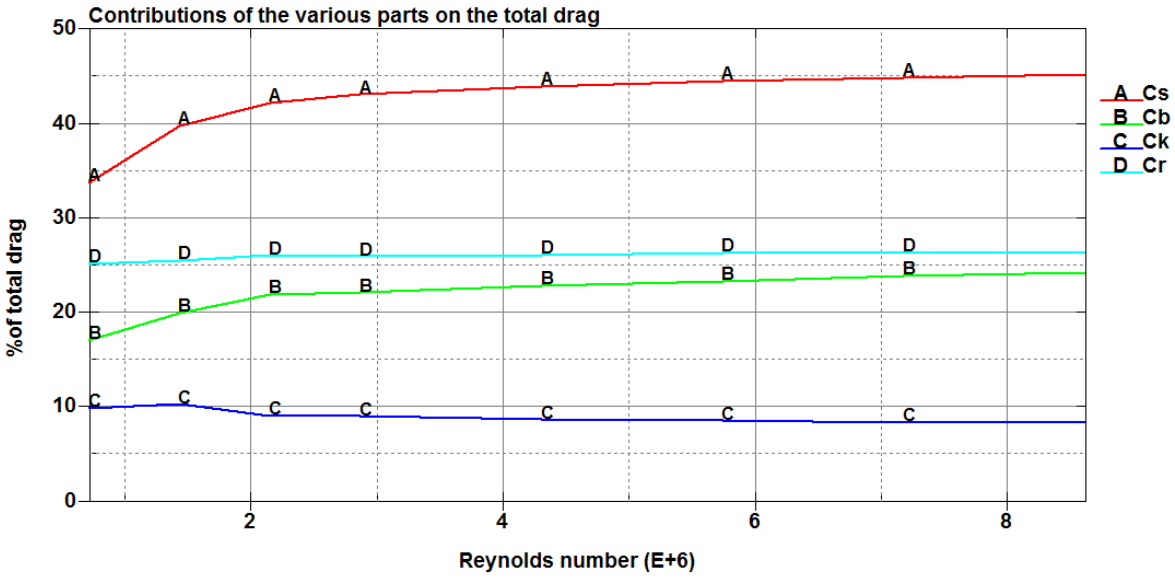

***Figure 14**: Contribution of the various parts on the total drag, Cs=slant drag, Cb=back drag, Ck=front drag, Cr=friction drag.*

4 Conclusion and future work

The usefulness of numeric analysis in general and the ICFD solver in particular has been demonstrated. Through a careful analysis of the available data, it was not only possible to validate the numerical results when compared to experiments but also to better explain the discrepancies that may exist between them. In future work, it would be interesting to try different slant angles and to try other turbulent models. Some other RANS models recently introduced in the ICFD solver ($k-\omega$, SST) but also the LES turbulence model. Finally, in a later stage, it would be interesting to come up with flexible flaps and structures to see if some drag reduction can be achieved this way and to make full use of the powerful FSI capabilities of LS-DYNA®.

5 Bibliography

Ahmed, S R, G Ramm, and G Faltin. *Some salient features of the time averaged ground vehicle wake.* Detroit: SAE Technical Paper Series 840300, 1984.

Bayraktar, Ilhan, Drew Landman, and Oktay Baysal. *Experimental and Computational Investigation of Ahmed Body for Ground Vehicle Aerodynamics.* Chicago: SAE Technical Paper Series, 2001.

Codina, Ramon. “Pressure Stability in Fractional Step Finite Element Methods for Incompressible Flows.” *Journal of Computational Physics* 170, no. 1 (2001): 112-140.

Conan, Boris, J. Anthoine, and P. Planquart. “Experimental Aerodynamic study of a car type bluff body.” *Experiments in fluids* 50 (2011): 1273-1284.

Del Pin, Facundo, Iñaki Çaldichoury, and Rodrigo Paz. *LS-DYNA ICFD Theory Manual.* LSTC, 2011.

Fourrie, Gregoire, Laurent Keirsbulck, Larbi Labraga, and Patrick Gillieron. “Bluff-body drag reduction using a deflector.” *Exp Fluids* 50 (2011): 385-395.

Franck, Gerardo, Norberto Nigro, Mario Storti, and Jorge D'Elia. “Numerical Simulation of the Flow around the Ahmed Vehicle Model.” Centro Internacional de Metodos Computacionales en Ingenierıa (CIMEC), n.d.

Gilleron, P, and E. Chometon. “Modelling of Stationary Three-Dimensional Separated air flows around an Ahmed reference model.” *ESAIM proc* 1999 (1999): 173-182.

Leclerc, Cedric. “Reduction de la trainee d'un vehicule automobile simplifie a l'aide du controle actif par jet synthetique.” PDH Thesis, Institut de Mecanique des fluides, Toulouse, 2008.

Lienhart, H, C. Stoots, and S. Becker. “Flow and Turbulence Structures in the Wake of a Simplified Car Model (Ahmed Modell).” In *New Results in Numerical and Experimental Fluid Mechanics III*, 323-330. n.d.

Meile, W, G Brenn, A. Reppenhagen, B. Lechner, and A. Fuchs. “Experiments and numerical simulations on the aerodynamics of the Ahmed body.” *CFD Letters* 3 (2011).

Shih, T.H, W.W. Liou, A. Shabbir, Z. Yang, and Zhu.J. “A New k-ε Eddy Viscosity Model for High Reynolds Number Turbulent Flows—Model Development and Validation.” *Computers Fluids* 24 (1995): 227-238.

Thacker, A., S. Aubrun, Leroy, and P. Devinant. “Effects of suppressing the 3D separation on the rear slant on the flow.” *Journal o fWind Engineering and Industrial Aerodynamics*, 2012: 237-243.

White, Frank M. *Fluid Mechanics 5th edition.* n.d.